JOURNAL OF GUIDANCE, CONTROL, AND DYNAMICS
Vol. 30, No. 5, September–October 2007

High-Altitude Satellite Relative Navigation Using Carrier-Phase Differential Global Positioning System Techniques

Shan Mohiuddin* and Mark L. Psiaki†
Cornell University, Ithaca, New York 14853-7501

DOI: 10.2514/1.27827

A new carrier-phase differential global positioning system relative navigation estimator has been developed that extends the use of carrier-phase differential global positioning system techniques to spacecraft formations that operate at geostationary altitudes and above. The estimator achieves rapid convergence to the carrier-phase ambiguities and incorporates a cycle slip detection and recovery algorithm. It solves a linearized problem using least-squares square-root information processing that does not require spacecraft dynamics models. In this context, integer ambiguities are resolved using an integer least-squares algorithm. The cycle slip algorithm identifies the slip channel by statistical hypothesis testing and estimates the magnitude of the slip. Global positioning system receiver-in-the-loop tests with simulated low-Earth orbit data show nearly instantaneous convergence to the correct integer ambiguities and relative position error magnitudes of less than 3 mm. Truth-model simulations are used to simulate geostationary orbits and high-Earth orbit scenarios. The geostationary orbit scenario produces nearly instantaneous convergence to the ambiguities and error magnitudes of less than 0.1 m. The high-Earth orbit case at a radial distance of 17.8 Earth radii converges in minutes with error magnitudes of less than 3 m. Cycle slips, present in the hardware-in-the-loop simulations, are detected and corrected without significant accuracy degradation.

Nomenclature

c	=	speed of light in a vacuum
$c\partial t$	=	increment to the pseudorange solution clock correction estimate
$\mathbf{e}$	=	extraction vector in the cycle slip detection algorithm
f_{L1}	=	$L1$ carrier signal nominal frequency
H	=	measurement sensitivity matrix
$\tilde{H}$	=	square-root information form of H
I	=	ionosphere error
$J(*)$	=	least-squares cost function
$J_{\text{res}}(*)$	=	least-squares residual cost function
$\mathbf{N}$	=	time-invariant double-differenced integer ambiguity vector
$\mathbf{N}_k$	=	time-varying integer ambiguity vector in the cycle slip recovery algorithm
$\hat{\mathbf{N}}_k$	=	time-varying integer ambiguity vector estimate in the cycle slip detection algorithm
$\mathbf{N}_{\text{opt}}$	=	optimal integer ambiguity vector solution
P	=	pseudorange measurement
Q	=	orthonormal transformation matrix
R	=	square-root information matrix
$R_{\nu\nu}$	=	inverse square root of the measurement error covariance matrix
$\mathbf{r}$	=	pseudorange position vector solution
$\hat{\mathbf{r}}_{AB}$	=	relative position vector estimate from receiver A to receiver B
t_A	=	receiver A time
$\mathbf{x}$	=	position/clock correction state vector
$\mathbf{x}_{\text{opt}}$	=	position/clock correction state vector estimate computed using $\mathbf{N}_{\text{opt}}$
$\mathbf{z}$	=	linearized measurement vector
$\hat{\mathbf{z}}$	=	factorized square-root information vector
$\tilde{\mathbf{z}}$	=	square-root information vector
$\mathbf{z}_{\text{res}}$	=	square-root information residual vector
γ	=	initial nominal phase in the receiver
Δn	=	integer cycle slip estimate
$\Delta\hat{n}$	=	real-valued cycle slip estimate
$\Delta(*)_{AB}$	=	single-differenced operator defined as $(*)_A - (*)_B$
$\delta\mathbf{r}$	=	absolute position correction vector
$\delta\mathbf{r}_{AB}$	=	relative position correction vector from receiver A to receiver B
δt	=	clock correction
δt_0	=	receiver clock correction computed in the pseudorange solution
λ_{L1}	=	$L1$ carrier signal nominal wavelength
ν	=	thermal and multipath noise vector
$\tilde{\nu}$	=	factorized square-root information noise vector
ρ	=	receiver/GPS-satellite range
$\hat{\rho}$	=	receiver/GPS-satellite line-of-sight unit vector
ρ_0	=	receiver/GPS-satellite range computed in the pseudorange solution
Σ	=	measurement error covariance matrix
ϕ	=	carrier-phase measurement
ψ	=	received carrier signal phase
ψ_0	=	initial nominal phase of the broadcast signal
$(*)_A$	=	quantities associated with receiver A
$(*)_{AB}$	=	differences of qualities associated with receivers A and B
$(*)_B$	=	quantities associated with receiver B
$(*)_P$	=	quantities associated with pseudorange measurements
$(*)_\phi$	=	quantities associated with carrier-phase measurements
$(*)^j$	=	quantities associated with satellite j or receiver channel j
$(*)^{ji}$	=	differences of quantities associated with satellite pair ji or receiver channel pair ji
$(*)^p$	=	quantities associated with cycle slip hypothesis p
$\nabla\Delta(*)^{ji}_{AB}$	=	double-differenced operator defined as $[(*)^j_A - (*)^j_B] - [(*)^i_A - (*)^i_B]$

Presented as Paper 6054 at the AIAA Guidance, Navigation, and Control Conference and Exhibition, San Francisco, CA, 15–18 August 2006; received 14 September 2006; revision received 26 April 2007; accepted for publication 30 April 2007.

*Graduate Student, Sibley School of Mechanical and Aerospace Engineering. Student Member AIAA.

†Professor, Sibley School of Mechanical and Aerospace Engineering. Associate Fellow AIAA.

I. Introduction

SPACECRAFT formation flying is a key technology for future space flight. For many new mission concepts, for example, NASA's magnetosphere multiscale mission [1], distributing the sensing over a formation offers both scientific and operational advantages over single-platform sensing. To achieve the benefits of distributed sensing, each spacecraft must have a high degree of autonomy, including the ability to autonomously navigate within the formation to a high degree of accuracy. Carrier-phase differential global positioning system (CDGPS) techniques are ideally suited for such accurate relative navigation. Low-Earth orbit (LEO) CDGPS systems have already produced cm- and sub-cm-level relative position accuracies using both simulated and flight data. The next step is to expand the application region to include geostationary orbits (GEO) and high-Earth orbits (HEO), both of which require the GPS receivers to operate above the GPS constellation. A CDGPS system operating in these high-altitude orbits must overcome poor visibility and poor geometric dilution of precision (GDOP), acquire and track very weak signals, and resolve carrier-phase measurement ambiguities with very slow receiver/GPS-satellite relative motion. Dual-frequency civilian technology may help solve these problems, but a practical system must be built upon a firm understanding of the capability of single-frequency CDGPS techniques. With this in mind, this paper examines and improves existing single-frequency CDGPS technology for space-based relative navigation.

An improved single-frequency system must make immediate use of newly acquired GPS signals, navigate continuously through periods of high GPS signal turnover, and detect and recover from carrier-phase cycle slips. These improvements are achievable with fast and reliable carrier-phase measurement ambiguity estimation techniques. Particular attention should be paid to incorporating double-differenced integer ambiguity resolution in an optimal manner. With the weaker observability of HEO and GEO systems, real-valued ambiguities would greatly increase the effective GDOP. This increase must be avoided because the systems are already challenged by poor geometry and noisy measurements. The proper use of double-differenced integer biases is, therefore, essential for successful high-altitude relative navigation systems.

Single-differenced CDGPS techniques, which result in real-valued ambiguities, have produced impressive accuracies in LEO simulations, often exhibiting 3-dimensional relative position errors of less than 3 mm over baseline distances of less than 10 km [2]. Double-differenced techniques have also proven accurate in LEO simulations, but some researchers have either estimated the double-differenced ambiguities as real numbers [3] or skirted the issue of how to begin the integer estimation process without a priori information [4]. These techniques are slow to converge and often retain uncertainty in the ambiguity estimates that can be eliminated by estimating the biases as exact integers. Other researchers have used optimal linear integer ambiguity estimation methods as part of dual-frequency CDGPS systems for LEO scenarios [5,6]. Such integer estimation methods are commonly called LAMBDA methods.[‡] All of these relative navigation estimators were designed to operate in LEO where the GPS receivers will experience relatively high carrier-to-noise ratios, good navigation geometry, and fast line-of-sight vector dynamics, all of which increase the observability of the integer ambiguities. The existing algorithms that implement LAMBDA solve the integer problem in the context of the normal estimation equations, an approach that may encounter numerical problems under certain circumstances, and they make use of dual-frequency measurements. The estimator in [5] attempts to handle carrier-phase cycle slips by implementing a detection scheme, but it is unclear how it would recover from such events.

[‡]Least-squares ambiguity decorrelation adjustment (LAMBDA) solves a linear least-squares problem under the condition that elements of the solution vector are all integers. The algorithm calculates the ambiguities very efficiently by decorrelating the highly correlated ambiguities before performing a search to find the minimum-cost vector estimate. The method is discussed further in Sec. IV.

The present effort seeks to expand the applicability of CDGPS techniques. It has been motivated by the conjecture that a properly posed estimation problem and a carefully designed solution algorithm that optimally integrates LAMBDA-type methods would be able to resolve the carrier-phase integer ambiguities in the challenging operating environments in GEO and HEO using $L1$ measurements only. Once resolved, the relative position estimation error would only depend on the carrier-phase measurement error and the GDOP, resulting in theoretical accuracies of about 0.1 m in GEO and about 2 m in HEO.

This paper makes two main contributions. First, it presents a single-frequency relative navigation estimator that optimally integrates LAMBDA-type integer ambiguity resolution techniques into its solution algorithm to resolve the carrier-phase biases in high-altitude orbits. The estimator solves a linearized problem with least-squares square-root information processing, which is appropriate for use with the square-root information LAMBDA techniques in [7]. The result is a simple formulation that does not require dynamics modeling, that is numerically stable, and that is easy to implement. The estimator's ability to navigate in high-altitude orbits in the presence of poor navigation geometry, weak ambiguity observability, and noisy measurements is demonstrated using a truth-model simulation. The second contribution is the inclusion in the estimator of a robust carrier-phase cycle slip detection and recovery algorithm that uses statistical hypothesis testing to identify which channel has slipped, estimates the number of cycles that have slipped on that channel, and ensures that the magnitude of the slip settles to an integer value before the estimator reverts back to normal operation. It accomplishes the recovery without discarding any measurements. The technique is developed in the square-root information (SRI) format and is easily transferable to SRI filtering.

The remainder of the paper is divided into the following six major sections. Section II presents the measurement models, discusses the elements of the carrier-phase model that are important to relative navigation, and explains the single- and double-differenced carrier-phase measurements. Section III describes the linearized relative navigation problem. Section IV derives the solution algorithm, focusing on how it takes full advantage of the integer ambiguity assumption. Section V develops the slip detection scheme and the recovery algorithm. Section VI presents the results from simulations. Section VII provides a summary of the work and a discussion of its conclusions.

II. Carrier-Phase Model and Measurement Equations

The carrier-phase model presented in [8] forms the basis for the relative navigation algorithm. That model considers how the carrier signals are generated at the transmitters and how they are measured at the receivers, with a special emphasis on how integer ambiguities arise in the context of CDGPS. Some of the relevant concepts are reviewed in this section, beginning with an overview of how a GPS receiver measures and reports carrier phase. In subsequent paragraphs, single- and double-differenced measurements are discussed, focusing on the nature of the measurement ambiguities.

A GPS receiver produces its carrier-phase measurement by computing a beat phase, which is the phase difference between a replica of the nominal $L1$ carrier signal and the received carrier as determined by a phase-lock loop (PLL). The replica signal's phase equals an initial value $\gamma^j_{A_0}$ plus a linear function of receiver time whose slope equals the nominal $L1$ carrier frequency f_{L1}. Suppose that the tracked phase of the received signal, generated by the PLL, is ψ^j. Then the beat phase model is

$$\phi^j_{A_k} = \gamma^j_{A_0} + f_{L1} t_{A_k} - \psi^j_{A_k} \tag{1}$$

Note that superscripts indicate the tracked GPS satellite and subscripts indicate a particular receiver (A or B) and the measurement sample index (k). The last term in Eq. (1), the received phase at time t_{A_k}, can be modeled by considering the carrier signal broadcast by the GPS satellite and the signal propagation time. The received signal's phase $\psi^j_{A_k}$ equals an initial transmitted phase ψ^j_0 plus a linear function

of the transmitter's clock time whose slope equals f_{L1}. This model is completed by considering the effects of the ionosphere, thermal noise, and most importantly, the difference between the receiver clock time and the transmitter clock time that is caused by the signal propagation time and the receiver and transmitter clock errors. Incorporating these terms into Eq. (1) and simplifying the expression yields the following carrier-phase measurement equation:

$$\phi^j_{A_k} = \underbrace{\gamma^j_{A_0} - \psi^j_0}_{\text{Ambiguity}} + f_{L1}(\delta t_{A_k} - \delta t^j_k) + \frac{1}{\lambda_{L1}}\rho^j_{A_k} - I^j_{A_k} - \nu^j_{\phi_{A_k}} \qquad (2)$$

In this equation, δt_{A_k} is the receiver clock error, δt^j_k is the satellite clock error, λ_{L1} is the nominal $L1$ carrier wavelength, $\rho^j_{A_k}$ is the receiver/GPS-satellite range, $I^j_{A_k}$ is an ionosphere effects term, and $\nu^j_{\phi_{A_k}}$ is the error caused by thermal noise and multipath. Notice how the measurement ambiguity is the difference between the initial phase of the receiver's nominal replica signal and the initial phase of the GPS-satellite broadcast signal. In general, there is no reason to believe that the initial phases would be integers. The measurement ambiguity, therefore, is a real number.

Single differencing of the measurements of two receivers tracking the same GPS satellite cancels out those terms that are common to that satellite, including the satellite broadcast signal's initial phase. It is assumed that the ionosphere errors are removed by this same process. For short baselines, this is a safe assumption because the line-of-sight vectors from the two receivers to a particular GPS satellite are nearly the same, resulting in ionosphere pierce points that are close to one another. For long baselines, this assumption breaks down. The subject of what to do for long baselines involves dual-frequency techniques that are beyond the scope of this paper. Please see [5] for more information on this topic. To simplify the notation, a single-differenced operator is defined as $\Delta(*)_{AB} = (*)_A - (*)_B$. Using this operator, the single-differenced carrier phase becomes

$$\Delta(\phi)^j_{AB_{kl}} = \underbrace{\gamma^j_{A_0} - \gamma^j_{B_0}}_{\Delta\text{Ambiguity}} + f_{L1}\Delta(\delta t)_{AB_{kl}} + \frac{1}{\lambda_{L1}}\Delta(\rho)^j_{AB_{kl}} - \Delta(\nu)^j_{\phi_{AB_{kl}}} \qquad (3)$$

The subscripts k and l indicates that the receiver measurement times t_{A_k} and t_{B_l} are not identical. If both receivers are applying their pseudorange-based navigation solution clock correction terms, however, these times will agree to within the uncertainties of those corrections, or within about 100 ns, when four or more satellites are tracked at each receiver. For readability, the k and l subscripts will be suppressed for the remainder of the paper.

Notice that the ambiguities in Eq. (3) are still real numbers because they are differences of the real-valued initial phases of the nominal carrier replica signals in the two receivers. If the receivers were operating on the same local oscillator and if the receiver line biases were calibrated out, then the single-differenced ambiguity would be an integer. These conditions are met in a typical attitude determination system, but in the case of relative navigation, the single-differenced ambiguities cannot be considered integers.

Taking single-differenced measurements for two different GPS satellites and differencing them produces a double-differenced measurement that cancels out those terms in Eq. (3) that are common to both receivers. The double-differenced operator is defined as $\nabla\Delta(*)^{ji}_{AB} = [(*)^j_A - (*)^j_B] - [(*)^i_A - (*)^i_B]$. Using this operator, the double-differenced phase is

$$\nabla\Delta(\phi)^{ji}_{AB} = \underbrace{\nabla\Delta(N)^{ji}_{AB}}_{\nabla\Delta\text{Ambiguity}} + \frac{1}{\lambda_{L1}}\nabla\Delta(\rho)^{ji}_{AB} + \nabla\Delta(\nu)^{ji}_{\phi_{AB}} \qquad (4)$$

If a receiver is properly designed, then each channel uses the same nominal carrier-phase replica to compute the beat carrier phase, or it uses a replica that differs from the others by an integer number of cycles. This fact causes each difference $\gamma^j_{A_0} - \gamma^i_{A_0}$ and $\gamma^j_{B_0} - \gamma^i_{B_0}$ to be an integer number of cycles. The double-differenced ambiguity $\nabla\Delta(N)^{ji}_{AB} = (\gamma^j_{A_0} - \gamma^i_{A_0}) - (\gamma^j_{B_0} - \gamma^i_{B_0})$ is thus guaranteed to be an integer. Manipulating the data to achieve integers increases measurement uncertainty and computational overhead, but the savings in convergence time and calculation time in estimating the ambiguities as exact integers justifies the losses. Furthermore, once the integers have been estimated and validated, the relative navigation estimator can treat them as exact values, allowing the precise carrier-phase measurements to be treated as though they were very accurate pseudorange-like measurements of the relative position. The integer nature of the double-differenced ambiguities features prominently in the posing of the relative navigation problem and in the derivation of the solution algorithm.

It is appropriate to comment here on how a GPS receiver should be set up to work with a CDGPS system. Each receiver should report pseudorange and carrier phase at its best estimate of the GPS second to ensure that the differencing operations do not introduce extra uncertainty as a result of large differences between the times t_{A_k} and t_{B_l}. Therefore, each receiver must produce an absolute navigation/clock solution and use the clock correction to guide its selection of sample times. Because it reports corrected times, the reported pseudorange must be modified to become $P_{\text{corr}} = P - c\delta t_0$, and the reported carrier phase must be modified to become $\phi_{\text{corr}} = \phi - f_{L1}\delta t_0$ [8,9]. Also, the availability of the pseudorange-based absolute solution for each receiver to the relative navigation system plays an important role in the linearization of the measurement equations.

III. Satellite Relative Navigation Problem

The target application for the present system is to achieve accurate relative navigation of two spacecraft in Earth orbit with arbitrary baseline distances. The algorithm must include fast ambiguity estimate convergence and reliable carrier-phase cycle slip detection and recovery. The system should operate with no a priori knowledge of position and velocity. The following steps are taken to realize this system: 1) pose the estimation problem and linearize it in such a way that the integer nature of the double-differenced carrier-phase ambiguities is preserved, and 2) derive a solution algorithm that will ensure rapid convergence to the correct integer ambiguities and that can take advantage of computationally efficient decorrelation and integer search algorithms.

The estimation problem is posed as a linearized least-squares problem so that, when the integer condition of the double-differenced carrier-phase integer ambiguities is imposed, it can be solved with existing linear integer estimation techniques like the LAMBDA method. The nonlinear measurement equations are linearized about the pseudorange solutions at each receiver independently. One consequence of this linearization is that the position correction variable can be separated into two vectors: an absolute position correction and a relative position correction. The resulting relative position corrections can be smaller than the position corrections found in other linearization schemes, resulting in a more accurate linearized model and a more accurate estimate. The advantages of this separation will be discussed in more detail in the derivation of the linearization and the solution algorithm.

The posing of the relative navigation problem begins with the pseudorange measurement equations for the two receivers. The derivation is presented for receiver A, but the same steps apply to the measurement equations for receiver B. The subscripts indicating the measurement times are suppressed to simplify the notation.

$$P^j_A = \rho^j_A + c\delta t_A - c\delta t^j + \nu^j_{P_A} \qquad (5)$$

P^j_A is the measured pseudorange, ρ^j_A is the true range, δt_A is the receiver clock error, δt^j is the satellite clock error, and $\nu^j_{P_A}$ is the error caused by thermal noise and multipath. Linearizing the equations about the pseudorange solution and grouping the known terms on the left and the linear unknown terms on the right gives

$$P^j_A - c\delta t_{A_0} + c\delta t^j - \rho^j_{A_0} = \left(\hat{\rho}^j_A\right)^T \delta\mathbf{r}_A + c\,\partial t_A + \nu^j_{P_A} \qquad (6)$$

The terms on the left side with subscript zero are the receiver clock correction and range computed by the pseudorange solution. On the right side, $\hat{\rho}_A^j$ is the unit direction vector that points from GPS satellite j to the pseudorange solution position for receiver A, $\delta\mathbf{r}_A$ is the absolute position correction vector to go from the pseudorange solution to the true position, and ∂t_A is the receiver clock correction increment to go from the pseudorange-based receiver clock correction to the true clock correction.

The CDGPS relative navigation algorithm uses modified unknowns to decompose the solution into a correction to the relative position, which it will determine precisely, and a correction to the absolute position. The receiver A absolute position correction vector can be represented as the sum of the receiver B absolute position correction vector $\delta\mathbf{r}_B$ and a relative position correction vector $\delta\mathbf{r}_{AB}$, thus separating the correction into two parts. A diagram of the change in unknowns is shown in Fig. 1, where $\mathbf{r}_{AB_0}$ is the differential position vector between the pseudorange solutions and $\mathbf{r}_{AB} = \mathbf{r}_{AB_0} + \delta\mathbf{r}_{AB}$ is the true differential position. The solution procedure will determine $\delta\mathbf{r}_{AB}$ and then add $\mathbf{r}_{AB_0}$ to it to compute $\mathbf{r}_{AB}$. Written in terms of these new unknowns, the linearized pseudorange equations for both receivers become

$$P_A^j - c\delta t_{A_0} + c\delta t^j - \rho_{A_0}^j = \left(\hat{\rho}_A^j\right)^T(\delta\mathbf{r}_B + \delta\mathbf{r}_{AB}) + c\partial t_A + \nu_{A_P}^j \quad (7)$$

$$P_B^j - c\delta t_{B_0} + c\delta t^j - \rho_{B_0}^j = \left(\hat{\rho}_B^j\right)^T\delta\mathbf{r}_B + c\partial t_B + \nu_{B_P}^j \quad (8)$$

The unknowns in the equations are $\delta\mathbf{r}_B$, $\delta\mathbf{r}_{AB}$, $c\partial t_A$, and $c\partial t_B$. If the carrier-phase data were not included, then the optimal solution for the quantities would be $\delta\mathbf{r}_B = \delta\mathbf{r}_{AB} = 0$ and $\partial t_A = \partial t_B = 0$. These would be the solutions because the pseudorange solutions already constitute the least-squares solutions to Eqs. (7) and (8) repeated for each tracked satellite.

The absolute position correction vector $\delta\mathbf{r}_B$ can be large, on the order of the single-frequency pseudorange solution error of about 10 m or more. By explicitly separating the absolute and relative position correction terms, the relative position correction $\delta\mathbf{r}_{AB}$ is insulated from the large absolute position uncertainty associated with the pseudorange measurements. The more accurate relative position correction is the part of the solution that is most affected by the addition of the carrier-phase measurements. Separating the variables in this way is not strictly necessary, but is instructive in the context of deriving and analyzing the estimator. The equations include receiver clock correction increments to account for any remaining errors that are common to all channels in each receiver.

The same linearization scheme is applied to the double-differenced carrier-phase equation, which yields

$$\lambda_{L1}\nabla\Delta(\phi)_{AB}^{ji} - \nabla\Delta(\rho)_{AB_0}^{ji} = \lambda_{L1}\nabla\Delta(N)_{AB}^{ji} + \left[\nabla\Delta(\hat{\rho})_{AB}^{ji}\right]^T\delta\mathbf{r}_B + \left(\hat{\rho}_A^j - \hat{\rho}_A^i\right)^T\delta\mathbf{r}_{AB} + \nabla\Delta(v)_{AB_\phi}^{ji} \quad (9)$$

Again, the absolute and relative correction terms are separated. This equation has been manipulated to group the known terms on the left and the linear unknown terms on the right. As in Eqs. (7) and (8), the unknown terms associated with the absolute and relative position corrections are $\delta\mathbf{r}_B$ and $\delta\mathbf{r}_{AB}$. The third unknown term is the double-differenced integer ambiguity $\nabla\Delta(N)_{AB}^{ji}$.

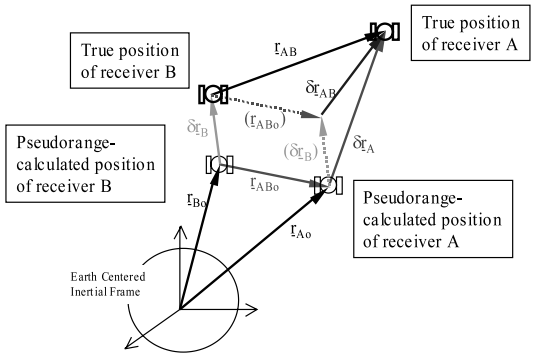

Fig. 1 Modified relative navigation unknowns.

IV. Solution Algorithm

The linearized measurement equations are set up to form a least-squares problem that allows pointwise solutions for the absolute position, relative position, and clock corrections, and that allows sequential solutions for the double-differenced integer ambiguities. The problem is solved with a square-root information estimator, which keeps track of the square root of the inverse of the ambiguity estimate covariance matrix. It carries this matrix forward, updating it at each time step, while solving from scratch for the updated relative and absolute positions at each time step. This type of estimator is typically called a real-time kinematic estimator. The square-root information form is numerically stable and suitable to work with the LAMBDA method. Both pseudorange and carrier-phase measurements are used in the solution. The inclusion of the pseudoranges limits the double-differenced carrier-phase ambiguity search volume to within the error of the pseudorange solution. This relatively small search volume is further reduced by the imposition of the integer condition, shrinking the set of candidates from all the possible combinations of real-valued ambiguities in the search volume to all the possible combinations of integer-valued ambiguities in the search volume. Only a few viable integer sets exist within the pseudorange-limited search volume. This reduced search volume will promote fast convergence to the correct bias estimates and, when coupled with the LAMBDA method, will promote fast calculation of the estimates.

The solution algorithm begins by combining linearized pseudorange and carrier-phase measurements into two matrix-vector equations. The pseudorange equation for the system is developed by repeating Eqs. (7) and (8) for all tracked GPS satellites from 1 to J:

$$\underbrace{\begin{bmatrix} z_{P_A}^1 \\ z_{P_A}^2 \\ \vdots \\ z_{P_A}^J \\ z_{P_B}^1 \\ z_{P_B}^2 \\ \vdots \\ z_{P_B}^J \end{bmatrix}}_{\mathbf{z}_{P_k}} = \underbrace{\begin{bmatrix} \left(\hat{\rho}_A^1\right)^T & \left(\hat{\rho}_A^1\right)^T & 1 & 0 & 0 & \cdots & 0 \\ \left(\hat{\rho}_A^2\right)^T & \left(\hat{\rho}_A^2\right)^T & 1 & 0 & 0 & \cdots & 0 \\ \vdots & \vdots & \vdots & \vdots & \vdots & \ddots & \vdots \\ \left(\hat{\rho}_A^J\right)^T & \left(\hat{\rho}_A^J\right)^T & 1 & 0 & 0 & \cdots & 0 \\ 0 & \left(\hat{\rho}_B^1\right)^T & 0 & 1 & 0 & \cdots & 0 \\ 0 & \left(\hat{\rho}_B^2\right)^T & 0 & 1 & 0 & \cdots & 0 \\ \vdots & \vdots & \vdots & \vdots & \vdots & \ddots & \vdots \\ 0 & \left(\hat{\rho}_B^J\right)^T & 0 & 1 & 0 & \cdots & 0 \end{bmatrix}}_{[H_{x_{P_k}}\ 0]} \begin{bmatrix} \mathbf{x}_k \\ \mathbf{N} \end{bmatrix} + \nu_{P_k} \quad (10)$$

where

$$\mathbf{x}_k = \begin{bmatrix} \delta\mathbf{r}_{AB_k} \\ \delta\mathbf{r}_{B_k} \\ c\partial t_{A_k} \\ c\partial t_{B_k} \end{bmatrix} \qquad \mathbf{N} = \begin{bmatrix} \nabla\Delta(N)_{AB}^{21} \\ \nabla\Delta(N)_{AB}^{31} \\ \vdots \\ \nabla\Delta(N)_{AB}^{J1} \end{bmatrix} \quad (11)$$

$$z_{P_A}^j = P_A^j - \rho_{A_0}^j + c(\delta t^j - \delta t_{A_0}) \quad (12)$$

$$z_{P_B}^j = P_B^j - \rho_{B_0}^j + c(\delta t^j - \delta t_{B_0}) \quad (13)$$

and ν_{P_k} is the pseudorange measurement noise vector. Note that $H_{x_{P_k}}$ consists of the first eight columns of the large matrix on the right-hand side of Eq. (10).

The carrier-phase equation for the system is developed by repeating Eq. (9) for all GPS-satellite pairs $ji = 21, 31, \ldots, J1$

$$\underbrace{\begin{bmatrix} z_{\phi_A}^{21} \\ z_{\phi_A}^{31} \\ \vdots \\ z_{\phi_A}^{J1} \end{bmatrix}}_{\mathbf{z}_{\phi_k}} = \underbrace{\begin{bmatrix} \left[\hat{\rho}_A^2 - \hat{\rho}_A^1\right]^T & \left[\nabla\Delta\left(\rho_{AB}^{21}\right)\right]^T & 0 & 0 & \lambda_{L1} & 0 & \cdots & 0 \\ \left[\hat{\rho}_A^3 - \hat{\rho}_A^1\right]^T & \left[\nabla\Delta\left(\rho_{AB}^{31}\right)\right]^T & 0 & 0 & 0 & \lambda_{L1} & \cdots & 0 \\ \vdots & \vdots & \vdots & \vdots & \vdots & \vdots & \ddots & \vdots \\ \left[\hat{\rho}_A^J - \hat{\rho}_A^1\right]^T & \left[\nabla\Delta\left(\rho_{AB}^{J1}\right)\right]^T & 0 & 0 & 0 & 0 & 0 & \lambda_{L1} \end{bmatrix}}_{[H_{x_{\phi_k}} H_{N_{\phi_k}}]} \begin{bmatrix} \mathbf{x}_k \\ \mathbf{N} \end{bmatrix} + \nu_{\phi_k} \tag{14}$$

where

$$z_\phi^{ji} = \lambda_{L1}\nabla\Delta(\phi)_{AB}^{ji} - \nabla\Delta\rho_{AB_0}^{ji} \tag{15}$$

and ν_{ϕ_k} is the carrier-phase measurement noise vector. The matrix $H_{x_{\phi_k}}$ consists of the first eight columns of the large matrix on the right-hand side of Eq. (14), and $H_{N_{\phi_k}}$ consists of the remaining $J-1$ columns.

The systems of linear equations in Eqs. (10) and (14) can be combined to yield

$$\begin{bmatrix} \mathbf{z}_{P_k} \\ \mathbf{z}_{\phi_k} \end{bmatrix} = \begin{bmatrix} H_{x_{P_k}} & 0 \\ H_{x_{\phi_k}} & H_{N_{\phi_k}} \end{bmatrix} \begin{bmatrix} \mathbf{x}_k \\ \mathbf{N} \end{bmatrix} + \begin{bmatrix} \nu_{P_k} \\ \nu_{\phi_k} \end{bmatrix} \tag{16}$$

The ambiguity vector $\mathbf{N}$ is assumed to be constant over all measurement epochs. This is only true if no carrier-phase cycle slips occur. These occurrences will instantly degrade the accuracy of the relative position estimate and must be detected before the estimator reports the degraded position corrections. Such a detection system is developed in the next section.

Because the ambiguities are constant in the absence of cycle slips, it is useful to carry information from one sample to the next. In fact, the estimation problem at sample k uses all available information about the ambiguities from samples 0 through $k-1$. This information takes the form of the square-root information equation $\hat{R}_{NN_{k-1}}\mathbf{N} = \hat{\mathbf{z}}_{N_{k-1}} - \nu_{N_{k-1}}$, where $\hat{\mathbf{z}}_{N_{k-1}}$ is the a priori information vector, $\nu_{N_{k-1}}$ is the associated zero-mean, unit-variance Gaussian noise vector, and $\hat{R}_{NN_{k-1}}$ is the a priori ambiguity square-root information matrix (SRIM). All the elements in $\hat{\mathbf{z}}_{N_{k-1}}$ and $\hat{R}_{NN_{k-1}}$ are initially set to zero for $k = 0$ to indicate that no a priori information is available. Augmenting the system in Eq. (16) with the a priori information gives

$$\begin{bmatrix} \mathbf{z}_{P_k} \\ \mathbf{z}_{\phi_k} \\ \hat{\mathbf{z}}_{N_{k-1}} \end{bmatrix} = \begin{bmatrix} H_{x_{P_k}} & 0 \\ H_{x_{\phi_k}} & H_{N_{\phi_k}} \\ 0 & \hat{R}_{NN_{k-1}} \end{bmatrix} \begin{bmatrix} \mathbf{x}_k \\ \mathbf{N} \end{bmatrix} + \begin{bmatrix} \nu_{P_k} \\ \nu_{\phi_k} \\ \nu_{N_{k-1}} \end{bmatrix} \tag{17}$$

Square-root information processing requires that the measurement equations be preconditioned to make their zero-mean, Gaussian errors have unit covariances. This conditioning involves left multiplication by a square root of the inverse covariance of the measurement errors in the original equations. The measurement error standard deviations are assumed to be $\sigma_P = 7$ m for the pseudorange measurements and $\sigma_\phi = 0.005$ m for the carrier-phase measurements. The pseudorange and carrier-phase measurements are independent on each channel, but when double differenced, the carrier-phase errors are not independent. The following are the measurement error covariance matrices and their square-root inverse factorizations for the pseudorange and double-differenced carrier-phase equations:

$$\Sigma_P = \sigma_P^2 \begin{bmatrix} 1 & 0 & \cdots & 0 \\ 0 & 1 & & \vdots \\ \vdots & & \ddots & \\ 0 & \cdots & & 1 \end{bmatrix} = R_{\nu\nu_P}^{-1}\left(R_{\nu\nu_P}^{-1}\right)^T \tag{18}$$

$$\Sigma_\phi = \sigma_\phi^2 \begin{bmatrix} 4 & 2 & \cdots & 2 \\ 2 & 4 & & \vdots \\ \vdots & & \ddots & \\ 2 & \cdots & & 4 \end{bmatrix} = R_{\nu\nu_\phi}^{-1}\left(R_{\nu\nu_\phi}^{-1}\right)^T \tag{19}$$

$R_{\nu\nu_P}$ equals σ_P^{-1} times an identity matrix and $R_{\nu\nu_\phi}$ can be computed from Σ_ϕ by inverting and transposing its Cholesky factorization. The problem is transformed to yield the desired square-root information form through left multiplication of the appropriate blocks by $R_{\nu\nu_P}$ and $R_{\nu\nu_\phi}$

$$\begin{bmatrix} \tilde{\mathbf{z}}_{P_k} \\ \tilde{\mathbf{z}}_{\phi_k} \\ \hat{\mathbf{z}}_{N_{k-1}} \end{bmatrix} = \begin{bmatrix} R_{\nu\nu_P}\mathbf{z}_{P_k} \\ R_{\nu\nu_\phi}\mathbf{z}_{\phi_k} \\ \hat{\mathbf{z}}_{N_{k-1}} \end{bmatrix} \tag{20}$$

$$\begin{bmatrix} \tilde{H}_{x_{P_k}} & 0 \\ \tilde{H}_{x_{\phi_k}} & \tilde{H}_{N_{\phi_k}} \\ 0 & \hat{R}_{NN_{k-1}} \end{bmatrix} = \begin{bmatrix} R_{\nu\nu_P}H_{x_{P_k}} & 0 \\ R_{\nu\nu_\phi}H_{x_{\phi_k}} & R_{\nu\nu_\phi}H_{N_{\phi_k}} \\ 0 & \hat{R}_{NN_{k-1}} \end{bmatrix} \tag{21}$$

$$\tilde{\nu}_k = \begin{bmatrix} R_{\nu\nu_P}\nu_{P_k} \\ R_{\nu\nu_\phi}\nu_{\phi_k} \\ \nu_{N_{k-1}} \end{bmatrix} \tag{22}$$

The solution algorithm then factorizes the coefficient matrix from Eq. (21) into the product of an orthonormal matrix and an upper-triangular matrix (QR factorization) [10,11]. The result is

$$Q_k \begin{bmatrix} \hat{R}_{xx_k} & \hat{R}_{xN_k} \\ 0 & \hat{R}_{NN_k} \\ 0 & 0 \end{bmatrix} = \begin{bmatrix} \tilde{H}_{x_{P_k}} & 0 \\ \tilde{H}_{x_{\phi_k}} & \tilde{H}_{N_{\phi_k}} \\ 0 & \hat{R}_{NN_{k-1}} \end{bmatrix} \tag{23}$$

where Q_k is an orthonormal matrix, $\hat{R}_{xx_k}$ is an 8×8 upper-triangular matrix, $\hat{R}_{NN_k}$ is a $(J-1) \times (J-1)$ upper-triangular matrix, and $\hat{R}_{xN_k}$ is an $8 \times (J-1)$ dense matrix. These matrices can be determined from the block matrix on the right-hand side of Eq. (23) using standard QR techniques. The measurement vector is transformed by left multiplying by the transpose of the Q_k matrix, giving

$$\begin{bmatrix} \hat{\mathbf{z}}_{x_k} \\ \hat{\mathbf{z}}_{N_k} \\ \mathbf{z}_{res_k} \end{bmatrix} = Q_k^T \begin{bmatrix} \tilde{\mathbf{z}}_{P_k} \\ \tilde{\mathbf{z}}_{\phi_k} \\ \hat{\mathbf{z}}_{N_{k-1}} \end{bmatrix} \tag{24}$$

resulting in the transformed block upper-triangular system

$$\begin{bmatrix} \hat{\mathbf{z}}_{x_k} \\ \hat{\mathbf{z}}_{N_k} \\ \mathbf{z}_{res_k} \end{bmatrix} = \begin{bmatrix} \hat{R}_{xx_k} & \hat{R}_{xN_k} \\ 0 & \hat{R}_{NN_k} \\ 0 & 0 \end{bmatrix} \begin{bmatrix} \mathbf{x}_k \\ \mathbf{N} \end{bmatrix} + \tilde{v}_k \tag{25}$$

where $\tilde{v}_k$ is a zero-mean, unit-variance noise vector.

At this point, estimates could be derived by setting $\tilde{v}_k$ to zero and solving for $\mathbf{x}_k$ and $\mathbf{N}$ by backsubstitution. This approach, however, ignores the fact that $\mathbf{N}$ is a vector of integers. To take advantage of this knowledge, an integer ambiguity resolution step is carried out before backsubstitution is used to determine $\mathbf{x}_k$. This resolution is accomplished by passing the decoupled ambiguity SRIM $\hat{R}_{NN_k}$ and the associated information vector $\hat{\mathbf{z}}_{N_k}$ to the LAMBDA solution algorithm.

The LAMBDA method is designed to produce viable integer ambiguity candidate vectors and to minimize a cost function to find the best vector. It solves the following integer linear least-squares (ILLS) problem: find $\mathbf{N}$ to minimize

$$J(\mathbf{N}) = \tfrac{1}{2}\left(\hat{R}_{NN_k}\mathbf{N} - \hat{\mathbf{z}}_{N_k}\right)^T \left(\hat{R}_{NN_k}\mathbf{N} - \hat{\mathbf{z}}_{N_k}\right) \tag{26}$$

under the condition that

$$\mathbf{N} \in Z^{J-1} \tag{27}$$

where Z^{J-1} indicates the space of $(J-1)$-dimensional integer vectors. The algorithm operates on the ambiguity SRIM $\hat{R}_{NN_k}$ using a unimodal linear transformation of the integers to approximately decorrelate the highly correlated ambiguities [7]. The transformed SRIM is passed to an integer search algorithm. That algorithm starts by generating a reasonable first guess of $\mathbf{N}_{\text{opt}}$, and it uses that guess to determine a cost that defines a bounded search volume. The algorithm finds all integer vectors inside the search volume, evaluates their costs, and designates the lowest cost vector as the correct ambiguity estimate.

The advantages of using this decorrelation and integer estimation algorithm are illustrated in Fig. 2. The upper plot shows the computed standard deviations for real-valued ambiguity estimates over a 600 s sample period. The standard deviations take more than 420 s to all drop below a unit value and would take more than 600 s to become small enough that the estimates could be safely rounded to the nearest integers. When the LAMBDA method is applied to this scenario, only a handful of valid integer ambiguity vectors are produced in the first time steps. After just 3 s, the number of valid candidates drops to 1, indicating to a high degree of probability that the correct integer vector has been identified. This behavior is indicated in the lower plot of Fig. 2. The LAMBDA method can resolve the ambiguities to their correct integer values 200 times faster than does an algorithm that estimates the ambiguities as real values and then rounds them to integers.

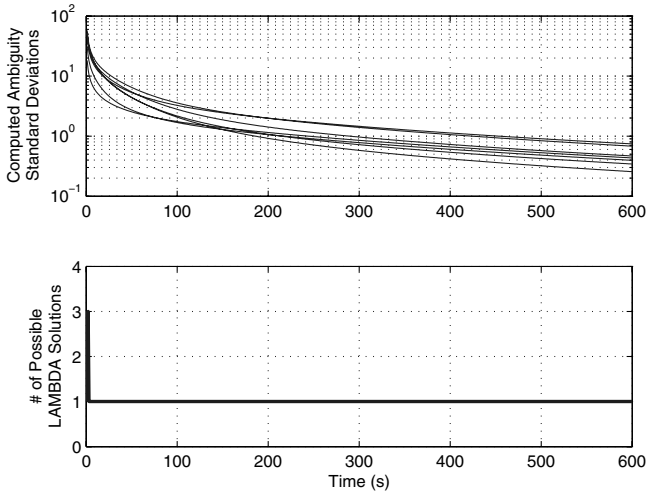

Fig. 2 Comparison of real-valued ambiguity convergence and the number of valid integer ambiguity vectors produced by the LAMBDA method.

Once the integer ambiguity vector $\mathbf{N}_{\text{opt}}$ has been estimated, it is passed back to the relative navigation estimator, which uses it to solve for the position corrections:

$$\mathbf{x}_{\text{opt}_k} = \hat{R}_{xx_k}^{-1}\left(\hat{\mathbf{z}}_{x_k} - \hat{R}_{xN_k}\mathbf{N}_{\text{opt}}\right) \tag{28}$$

To complete the algorithm's recursion, the square-root information vector associated with the ambiguities $\hat{\mathbf{z}}_{N_k}$ and the ambiguity SRIM $\hat{R}_{NN_k}$ is passed forward to sample index $k+1$ as a priori information.

The executive solution algorithm is summarized in the following steps:

1) Set counter $k = 0$ and set diffuse prior for the ambiguity estimate SRIM $\hat{R}_{NN_k} = 0$ and the vector $\hat{\mathbf{z}}_k = 0$.

2) Update counter $k = k + 1$, calculate the pseudorange solution, derive quantities for the transformed linearized measurement equations that appear in Eqs. (20) and (21), and QR factorize the problem as in Eqs. (23) and (24) to produce blocks for position corrections and ambiguity estimates.

3) Check for cycle slips. (The method for detecting cycle slips is described in the next section.) If yes, then apply the slip recovery algorithm (also described in the next section). If no, continue.

4) Solve the ILLS problem associated with Eq. (26) to determine $\mathbf{N}_{\text{opt}}$.

5) Solve for position/clock corrections using Eq. (28) and add a relative position correction to the relative position estimate calculated by differencing the pseudorange solution absolute positions.

$$\hat{\mathbf{r}}_{AB_k} = \mathbf{r}_{A_{P_k}} - \mathbf{r}_{B_{P_k}} + \delta r_{AB_k} \tag{29}$$

6) Retain ambiguity SRIM $\hat{R}_{NN_k}$ and the vector $\hat{\mathbf{z}}_{N_k}$. Go to step 2.

V. Cycle Slip Detection and Recovery

The estimation process in the executive algorithm breaks down when the PLL of one of the receivers' channels produces a carrier-phase jump, commonly called a cycle slip. In this paper, the term carrier-phase measurement jump and carrier-phase cycle slip have similar meanings. The distinction, where applicable, is that a jump may not be an exact integer number of cycles. The term cycle slip tends to imply an integer number. A well-designed receiver will experience few jumps, and the jumps will have noninteger values only during brief transients. After the transients, the slip stabilizes at a constant, exact integer.

Because the ambiguity estimates should be constant, a cycle slip is caught by looking for discrepancies between the a priori information and the current measurements. Such discrepancies appear as large jumps in the cost associated with the measurement residuals. Once the cost exceeds a threshold, the algorithm enters the cycle slip recovery (CSR) mode. In this mode, it performs hypothesis testing to identify the slip channel, and it estimates the number of cycles that have slipped on that channel. Measurement errors of this type usually occur over several time steps, and although the errors will ultimately settle to integer numbers of cycles, they are treated as real numbers during the transients. Once the cycle slip estimate has converged to an integer, the algorithm reverts to the normal mode of operation.

The residual cost that is an indicator of measurement errors is defined as

$$J_{\text{res}} = \tfrac{1}{2}\left(\hat{R}_{NN_k}\mathbf{N}_{\text{opt}} - \hat{\mathbf{z}}_{N_k}\right)^T \left(\hat{R}_{NN_k}\mathbf{N}_{\text{opt}} - \hat{\mathbf{z}}_{N_k}\right) + \tfrac{1}{2}\mathbf{z}_{\text{res}_k}^T \mathbf{z}_{\text{res}_k} \tag{30}$$

where the first term on the right-hand side is the optimal LAMBDA cost from Eq. (26) and the second term is the cost associated with the residual least-squares error vector $\mathbf{z}_{\text{res}_k}$ from Eq. (24). The quantity $2J_{\text{res}}$ should be distributed like a chi-squared distribution of degree $4J - 10$, provided there are no cycle slips. This distribution can be used to calculate a cost threshold that will indicate phase jumps. The calculation is carried out by solving an inverse cumulative distribution function with a user-specified false alarm probability. For a particular scenario, a reasonable false alarm probability results in a cost threshold of 30. Figure 3 shows typical cost values during good measurements and the increment in cost that occurs at a cycle slip.

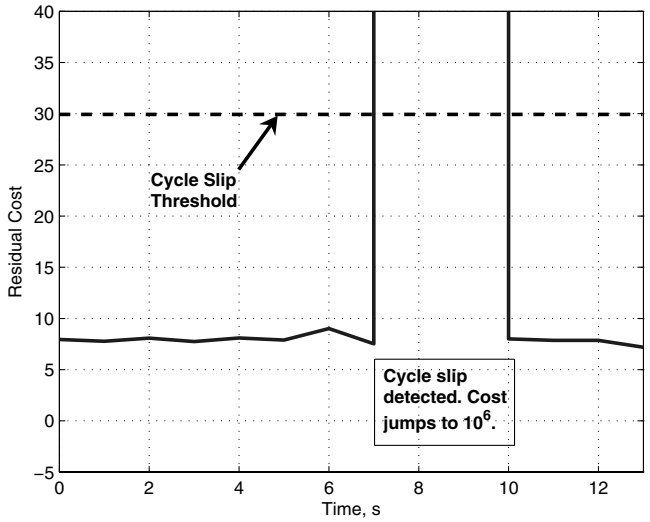

Fig. 3 Residual cost and cycle slip detection threshold cost.

Once a cycle slip is detected, the algorithm saves the last good ambiguity estimate as $\mathbf{N}_{\text{old}}$ for later comparison and then attempts to isolate the channel on which the error occurred. It does this by testing multiple hypotheses. Each hypothesis assumes that a different channel has slipped. To this end, a new ambiguity vector is defined as

$$\mathbf{N}_{\text{new}} = \mathbf{N}_{\text{old}} + \mathbf{e}^p \Delta n_k^p \tag{31}$$

where $p = 1, 2, \ldots, J$ indicates the assumed slip channel, and $\mathbf{e}^p$ is an $(J-1) \times 1$ vector defined as

$$\mathbf{e}^1 = \begin{bmatrix} -1 \\ -1 \\ -1 \\ \vdots \\ -1 \end{bmatrix} \mathbf{e}^2 = \begin{bmatrix} 1 \\ 0 \\ 0 \\ \vdots \\ 0 \end{bmatrix}, \mathbf{e}^3 = \begin{bmatrix} 0 \\ 1 \\ 0 \\ \vdots \\ 0 \end{bmatrix}, \ldots, \mathbf{e}^J = \begin{bmatrix} 0 \\ 0 \\ 0 \\ \vdots \\ 1 \end{bmatrix} \tag{32}$$

The first vector indicates that the cycle slip occurred in the single-differenced measurement that has been subtracted off of all of the other single-differenced measurements as part of the double-differenced data manipulation. Based on the definitions in Eq. (11), this is considered to be the $p = 1$ channel of the receiver. For simplicity, the measurement blocks defined in Eq. (23) are redefined in more compact notation here.

$$\tilde{H}_{mx_k} = \begin{bmatrix} \tilde{H}_{x_{P_k}} \\ \tilde{H}_{x_{\phi_k}} \end{bmatrix}; \qquad \tilde{H}_{mN_k} = \begin{bmatrix} 0 \\ \tilde{H}_{N_{\phi_k}} \end{bmatrix} \tag{33}$$

The measurement block associated with the position correction estimate R_{mx_k} is QR factorized

$$Q_{x_k} \begin{bmatrix} R_{xx_k} \\ 0 \end{bmatrix} = \tilde{H}_{mx_k} \tag{34}$$

and the problem is transformed

$$\begin{bmatrix} R_{xN_k} \\ R_{aN_k} \end{bmatrix} = Q_{x_k}^T \tilde{H}_{mN_k} \tag{35}$$

$$\begin{bmatrix} \mathbf{z}_{x_k} \\ \mathbf{z}_{a_k} \end{bmatrix} = Q_{x_k}^T \begin{bmatrix} \tilde{\mathbf{z}}_{P_k} \\ \tilde{\mathbf{z}}_{\phi_k} \end{bmatrix} \tag{36}$$

The problem is now ready for sequential hypothesis testing. If there were no cycle slips, then the information equations for $\mathbf{N}$ would take the form

$$\begin{bmatrix} R_{aN_k} \\ \hat{R}_{NN_{k-1}} \end{bmatrix} \mathbf{N} = \begin{bmatrix} \mathbf{z}_{a_k} \\ \hat{\mathbf{z}}_{N_{k-1}} \end{bmatrix} \tag{37}$$

The pth cycle slip hypothesis is that the first row of this system should be modified to be $R_{aN_k}[\hat{\mathbf{N}}_k^p + \mathbf{e}^p \Delta \hat{n}_k^p] = \mathbf{z}_{a_k}$, while the second row remains $\hat{R}_{NN_{k-1}} \hat{\mathbf{N}}_k^p = \hat{\mathbf{z}}_{N_{k-1}}$, where $\hat{\mathbf{N}}_k^p$ should be $\mathbf{N}_{\text{old}}$, and where $\Delta \hat{n}_k^p$ should be the slip magnitude. Rewritten in block form, these equations become

$$\begin{bmatrix} R_{aN_k} \mathbf{e}^p & R_{aN_k} \\ 0 & \hat{R}_{NN_{k-1}} \end{bmatrix} \begin{bmatrix} \Delta \hat{n}_k^p \\ \hat{\mathbf{N}}_k^p \end{bmatrix} = \begin{bmatrix} \mathbf{z}_{a_k} \\ \hat{\mathbf{z}}_{N_{k-1}} \end{bmatrix} \tag{38}$$

QR factorization is applied to the augmented matrix to isolate the blocks associated with $\Delta \hat{n}_k^p$ and $\hat{\mathbf{N}}_k^p$

$$Q_{N_k}^p \begin{bmatrix} R_{\Delta n \Delta n_k}^p & R_{\Delta n N_k}^p \\ 0 & \hat{R}_{NN_k}^p \end{bmatrix} = \begin{bmatrix} R_{aN_k} \mathbf{e}^p & R_{aN_k} \\ 0 & \hat{R}_{NN_{k-1}} \end{bmatrix} \tag{39}$$

and again the nonhomogeneous term is also transformed

$$\begin{bmatrix} z_{\Delta n_k}^p \\ \hat{\mathbf{z}}_{N_k}^p \end{bmatrix} = (Q_{N_k}^p)^T \begin{bmatrix} \mathbf{z}_{a_k} \\ \hat{\mathbf{z}}_{N_{k-1}} \end{bmatrix} \tag{40}$$

The transformed quantities $\hat{R}_{NN_k}^p$ from the second row of Eq. (39) and $\hat{\mathbf{z}}_{N_k}^p$ from the second row of Eq. (40) are then passed to the LAMBDA integer estimation algorithm, which minimizes the following cost function:

$$J\left(\hat{\mathbf{N}}_k^p\right) = \tfrac{1}{2}\left(\hat{R}_{NN_k}^p \hat{\mathbf{N}}_k^p - \hat{\mathbf{z}}_{N_k}^p\right)^T \left(\hat{R}_{NN_k}^p \hat{\mathbf{N}}_k^p - \hat{\mathbf{z}}_{N_k}^p\right) \tag{41}$$

Equations (38–41) are evaluated for $p = 1, 2, \ldots, J$. The minimum-cost solution indicates the cycle slip channel.

The next step is to calculate the number of cycles slipped under the assumption that the receiver may temporarily slip a noninteger number of cycles. The real-valued cycle slip variable $\Delta \hat{n}_k^p$ is calculated using the remaining blocks from Eqs. (39) and (40), setting $\hat{\mathbf{N}}_{\text{opt}_k} = \hat{\mathbf{N}}_{\text{opt}_k}^p$ for the p value associated with the correct slip channel assumption. At this point, all the p superscripts can be dropped, because the algorithm will use the minimum-cost p value.

$$\Delta \hat{n}_k = R_{\Delta n \Delta n_k}^{-1} \left[z_{\Delta n_k} - R_{\Delta n N_k} \hat{\mathbf{N}}_{\text{opt}_k} \right] \tag{42}$$

The position corrections are calculated using $\Delta \hat{n}_k$, $\hat{\mathbf{N}}_{\text{opt}_k}$, and the appropriate quantities from Eqs. (34–36)

$$\mathbf{x}_{\text{opt}_k} = R_{xx_k}^{-1} \left[\mathbf{z}_{x_k} - R_{xN_k} \left(\hat{\mathbf{N}}_{\text{opt}_k} + \mathbf{e}^p \Delta \hat{n}_k \right) \right] \tag{43}$$

The CSR algorithm then assembles a larger cost function

$$J(\Delta n_k, \mathbf{N}_k) = \frac{1}{2} \left(\begin{bmatrix} R_{\Delta n \Delta n_k} & R_{\Delta n N_k} \\ 0 & \hat{R}_{NN_k} \end{bmatrix} \begin{bmatrix} \Delta n_k \\ \mathbf{N}_k \end{bmatrix} - \begin{bmatrix} z_{\Delta n_k} \\ \mathbf{z}_{N_k} \end{bmatrix} \right)^T \left(\begin{bmatrix} R_{\Delta n \Delta n_k} & R_{\Delta n N_k} \\ 0 & \hat{R}_{NN_k} \end{bmatrix} \begin{bmatrix} \Delta n_k \\ \mathbf{N}_k \end{bmatrix} - \begin{bmatrix} z_{\Delta n_k} \\ \mathbf{z}_{N_k} \end{bmatrix} \right) \tag{44}$$

where Δn_k is a cycle slip variable that is constrained to be an integer, and where $\mathbf{N}_k$ is a time-varying integer ambiguity vector. This problem is solved using the LAMBDA method. Continuing under the assumption that the number of cycles slipped may not be an integer number of cycles during a multiple time step disruption, these solutions from LAMBDA are not used for the navigation solution, but are saved for comparison in the subsequent time steps.

The algorithm passes $\hat{R}_{NN_k}$ and $\hat{\mathbf{z}}_{N_k}$ forward to the next time step as a priori information, and repeats the CSR steps outlined above. This time, however, it uses the cycle slip channel estimate from the previous time step instead of searching through all the channel hypotheses. The stopping criterion for the CSR algorithm is that the integer cycle slip determined by minimizing the cost function in Eq. (44) remains unchanged for one time step, thatis, $\Delta n_{\text{opt}_k} = \Delta n_{\text{opt}_{k-1}}$, and that the integer ambiguity vector estimate from time k equals the ambiguity vector estimate from just before the cycle slip, that is, $\mathbf{N}_{\text{opt}_k} = \mathbf{N}_{\text{old}}$.

At this point, the CSR algorithm must perform some manipulations to pass the appropriate a priori information to the

executive estimator. It recognizes that the new a priori square-root information equation for the ambiguities should be equivalent to

$$\begin{bmatrix} R_{\Delta nN_k} \\ R_{NN_k} \end{bmatrix} \mathbf{N}_{\text{old}} = \begin{bmatrix} R_{\Delta nN_k} \\ R_{NN_k} \end{bmatrix} \{\mathbf{N}_{\text{new}} - \mathbf{e}^p \Delta n_{\text{opt}_k}\} = \begin{bmatrix} z_{\Delta n_k} - R_{\Delta n \Delta n_k} \Delta n_{\text{opt}_k} \\ \hat{\mathbf{z}}_{N_k} \end{bmatrix} - \begin{bmatrix} v_{\Delta n_k} \\ \hat{v}_{N_k} \end{bmatrix} \tag{45}$$

It QR factorizes the coefficient matrix of $\mathbf{N}_{\text{new}}$

$$\bar{Q}_{N_k} \begin{bmatrix} \bar{R}_{NN_k} \\ 0 \end{bmatrix} = \begin{bmatrix} R_{\Delta nN_k} \\ \hat{R}_{NN_k} \end{bmatrix} \tag{46}$$

and collects and transforms the equation's nonhomogeneous terms

$$\begin{bmatrix} \bar{\mathbf{z}}_{N_k} \\ \bar{\mathbf{z}}_{r_k} \end{bmatrix} = \bar{Q}_{N_k}^T \begin{bmatrix} \{z_{\Delta n_k} - R_{\Delta n \Delta n_k} \Delta n_{\text{opt}_k} + R_{\Delta nN_k} \mathbf{e}^p \Delta n_{\text{opt}_k}\} \\ \{\mathbf{z}_{N_k} + R_{NN_k} \mathbf{e}^p \Delta n_{\text{opt}_k}\} \end{bmatrix} \tag{47}$$

It then sets $\hat{R}_{NN_{k-1}} = \bar{R}_{NN_k}$ and $\hat{\mathbf{z}}_{N_{k-1}} = \bar{\mathbf{z}}_{N_k}$, and returns to the original solution algorithm.

The cycle slip recovery algorithm is illustrated in block diagram form in Fig. 4 and is summarized in the following steps:

1) Save the integer ambiguity estimate calculated just before the cycle slip, that is, $\mathbf{N}_{\text{old}} = \mathbf{N}_{\text{opt}}$.

2) Perform hypothesis testing by optimizing the cost in Eq. (41) for each channel. Let the slip channel be called channel p.

3) Calculate/retain the integer ambiguity estimate $\hat{\mathbf{N}}_k^p$ associated with the slip channel.

4) Calculate the real-valued number of cycles that have slipped $\Delta\hat{n}_k^p$ using Eq. (42) and calculate the position corrections $\mathbf{x}_k$ using Eq. (43).

5) Use the LAMBDA method to determine the minimizing integer values Δn_k and $\mathbf{N}_k$ associated with the cost in Eq. (44).

6) Set $k = k + 1$, retrieve new measurements, perform transformations in Eqs. (34–36), repeat steps 3, 4, and 5, then continue to step 7.

7) Check if $\Delta n_{\text{opt}_k} = \Delta n_{\text{opt}_{k-1}}$ and if $\mathbf{N}_{\text{opt}_k} = \mathbf{N}_{\text{old}}$. If both conditions are satisfied, go to step 8. If either condition is not satisfied, set $k = k + 1$, retrieve new measurements, perform transformations in Eqs. (34–36), and repeat steps 3, 4, 5, and 7.

8) Calculate the appropriate a priori information using Eqs. (47) and (48), and return to step 2 of the executive solution algorithm.

VI. Results from Hardware Receiver/Simulator Data and Off-Line MATLAB Simulator Data

Evaluation of a spacecraft relative navigation estimator requires the use of sophisticated simulations and space-qualified GPS receivers. A state-of-the-art GPS simulation laboratory exists at NASA Goddard Space Flight Center in the formation flying testbed (FFTB). This laboratory includes a multichannel satellite navigation simulator capable of replicating the GPS RF signals that would be received by antennas onboard orbiting platforms [12]. A receiver connected to the simulator behaves as if it were onboard an actual spacecraft (except for the environmental effects such as radiation and temperature extremes). A commercial-off-the-shelf (COTS) GPS receiver will not navigate under these conditions due to government-imposed altitude and speed restrictions. Dedicated space-qualified receivers must be used instead, and such receivers, designed by the German space agency DLR, are available at the FFTB. The Orion receivers were designed specifically for use in satellite formation flying. They were built using a COTS chipset and software package, but they include significant software modifications to ensure that they measure and report carrier-phase data correctly [13].

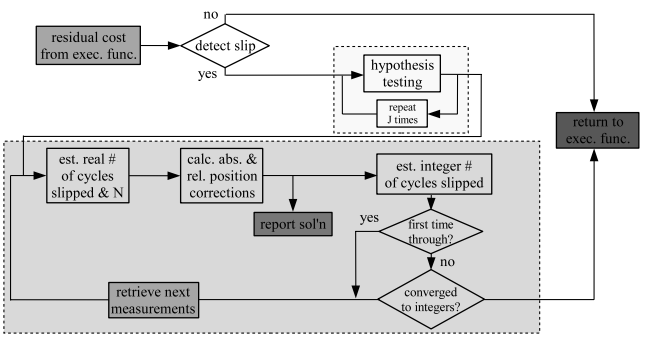

Fig. 4 Cycle slip recovery algorithm.

The signal simulator and the DLR Orion receivers have been used to replicate on-orbit relative navigation CDGPS measurements. The data have simulated a 2-spacecraft, 1-km-baseline formation in LEO. Ionosphere and multipath errors have not been simulated to obtain a measure of the relative navigation estimator's baseline performance under idealized conditions. These results have been used to compare the new algorithm's performance in LEO scenarios to previous work. Using these data, the algorithm typically converges to the correct integer ambiguities in 1–2 one-second time steps and reaches a probability that the estimated integers are the correct integers of 0.99 in 3–4 time steps when tracking eight or more GPS satellites. The probability calculation is based on the Bayesian analysis method presented in [7]. It calculates the probability that the integer estimates are correct conditioned on the data and on the a priori ambiguity information according to the following formula:

$$P(\mathbf{N}_{\text{opt}} | \hat{\mathbf{z}}_N) = \frac{\exp[-J(\mathbf{N}_{\text{opt}})]}{\sum_{m=1}^{M} \exp[-J(\mathbf{N}_m)]} \tag{48}$$

where $\mathbf{N}_m$ for $m = 1, 2, \ldots, M$ constitutes the set of all remotely possible integer vectors determined by the LAMBDA/ILLS algorithm. The size of this set and, correspondingly, the upper limit M of the summation in the denominator of Eq. (48) are chosen to be large enough that the summation approximates the infinite sum required by the Bayesian analysis.

A comparison between the relative position estimates and the true relative positions that are available from the signal simulator has found 3-dimensional relative position errors of 3 mm. Figure 5 shows about 200 s of the estimated baseline distance and the true baseline distance for a typical test case. In this case, and many others, the correct integer ambiguities were estimated in the first time step. Figure 6 plots the position error magnitude time history of the same sample period. These accuracies, achieved using $L1$-only measurements, are similar to those achieved by previous dual-frequency estimators that incorporate LAMBDA and the convergence times are faster [5,6], although a direct comparison is not valid given the idealized conditions of the simulation.

The estimator has been tested under GEO and HEO scenarios using data that have been generated by an off-line MATLAB truth-model simulation. This simulator is described in detail in [8] and includes realistic error models. The effects of the ionosphere are simulated using a modified version of the standard GPS broadcast

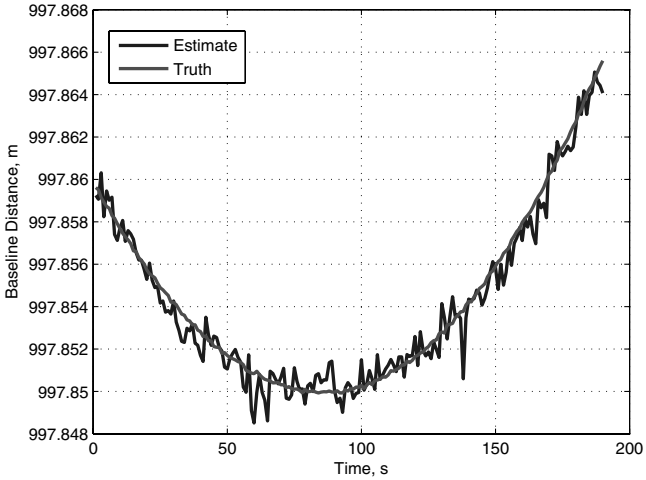

Fig. 5 1-km-baseline, LEO scenario. Estimated and true baseline distance.

model that incorporates altitude dependence into its electron density model. The total electron content for each channel is calculated by numerically integrating along the line-of-sight (LOS) vectors. The multipath error is modeled as being a function of the LOS directions to each GPS satellite as measured with respect to each user spacecraft's body coordinates. This function is implemented using a spherical harmonic expansion, allowing the model to capture the local azimuth and elevation dependencies of the multipath errors. The model assumes that the user spacecraft are relatively small and simple, having no large appendages. It would not be valid for large, complex spacecraft, for example, the International Space Station. The maximum carrier-phase multipath error is 5 mm. These detailed error models allow the simulator to replicate the expected real-world conditions a receiver would experience at high altitudes.

A representative GEO scenario consists of a 2-spacecraft formation with a 3 km baseline. It is assumed that the receivers include the weak-signal acquisition and tracking algorithms described in [14,15] that allow the use of the very weak side lobes of the GPS satellites' broadcast beams. Under the assumption that signals can be tracked down to $C/N_0 = 18$ dB · Hz, receivers in GEO can track up to 11 GPS signals with a GDOP of between 5 and 13. For scenarios where eight or more GPS satellites are tracked and where the GDOP is less than 12, the algorithm converges to the correct integer ambiguities in 1–2 30-second time steps and reaches 99% certainty in 3–4 time steps. It produces relative position error magnitudes of less than 0.1 m. Figure 7 shows the time histories of the position error components for this case.

A representative HEO scenario places the spacecraft in a 1.2×18 Earth radii orbit with a baseline of 10 km at apogee. In this scenario, it is assumed that the receivers can track signals down to $C/N_0 = 12$ dB · Hz. This threshold allows each receiver to track up to nine satellites at apogee with a GDOP between 110 and 300. In a scenario where seven or more GPS satellites are tracked and where the GDOP is less than 250, the algorithm converges to the correct integer ambiguities in 6–7 30-second time steps and reaches 99% certainty in 9–10 time steps. It produces relative position errors of less than 3 m. Figure 8 shows the time histories of the position error components for this case. Notice that the most significant errors occur in the weakly observable radial direction. Errors in this direction might be reducible by the addition of spacecraft relative dynamics to the solution algorithm through filtering, although this improvement would come at the cost of added complexity.

The hardware-in-the-loop data sets collected with the Orion receivers and the FFTB simulators included many carrier-phase jumps and offered an opportunity to test the cycle slip detection and recovery system. Given that the estimator typically converges to the correct integer ambiguities in 1–2 one-second time steps with no a priori information, a reasonable alternative approach to this paper's cycle slip recovery system would be to set the uncertainties associated with the ambiguity estimates to very large numbers after a cycle slip is detected, essentially resetting the estimator. This ad hoc method produces a jump in the relative position error on the order of several meters, as illustrated in Fig. 9. The new CSR algorithm improves the estimator's transient performance during slips. Figure 10 shows the error magnitude time history for the same block of data shown in Fig. 9, but for an estimator that uses the new slip recovery algorithm. The cycle slip detection and recovery system correctly detects a measurement error and correctly identifies the channel on which the slip occurred. The estimate of the number of cycles slipped converges to an integer in three 1-second time steps. During convergence, the relative navigation solution, calculated with the real-valued cycle slip variable, shows no significant accuracy degradation.

Note that the cycle slip detection and recovery algorithm has been tested only in LEO. It is expected to show similarly good performance in GEO because of the demonstrated ability to rapidly resolve ambiguities at those altitudes, even without a priori information. Performance in HEO may be less robust because ambiguity resolution takes longer at those altitudes.

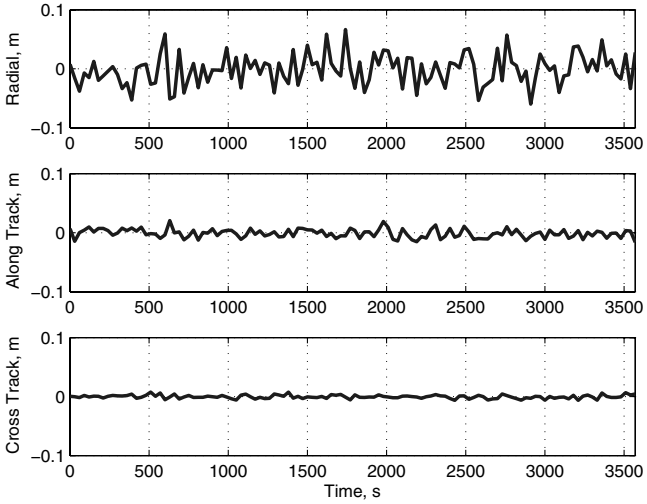

Fig. 7 Time histories of the relative position error components for a geostationary formation.

VII. Conclusions

A new satellite relative navigation estimator has been developed. It incorporates integer ambiguity resolution in an optimal manner.

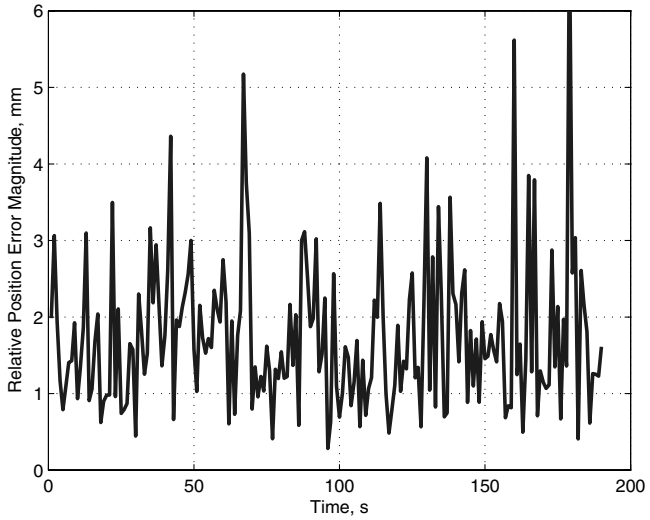

Fig. 6 1-km-baseline, LEO scenario. Time history of the relative position error magnitude.

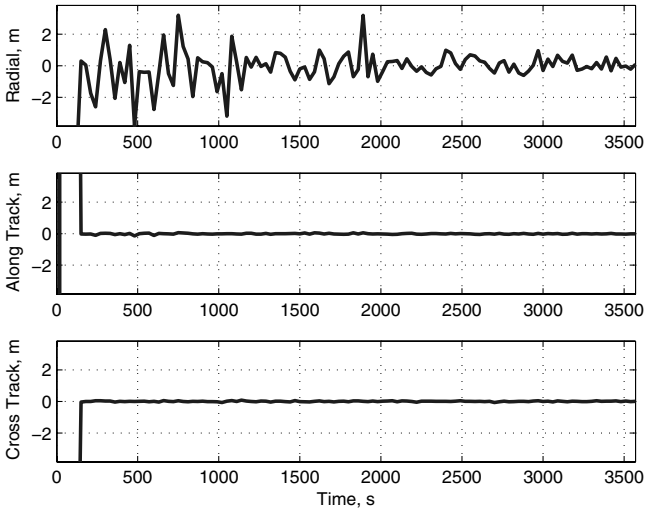

Fig. 8 Time histories of the relative position error components for a formation in a 1.2×18 Earth radii orbit when at a radial distance of 17.8 Earth radii.

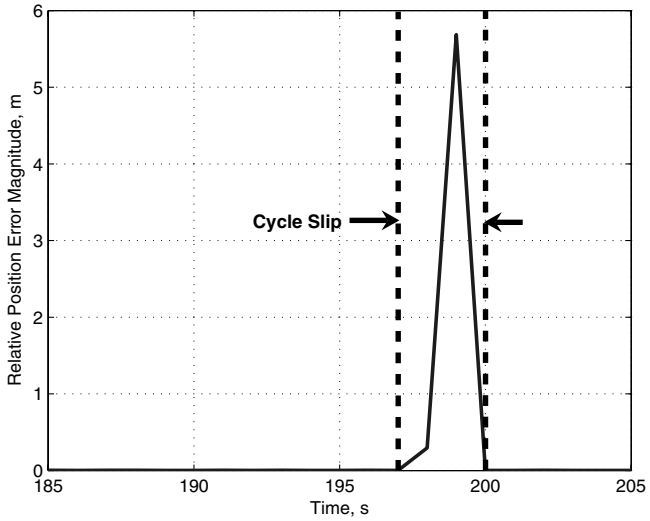

Fig. 9 Time history of the relative position error magnitude during a cycle slip event when using an ad hoc approach that discards all a priori ambiguity information at the onset of the slip.

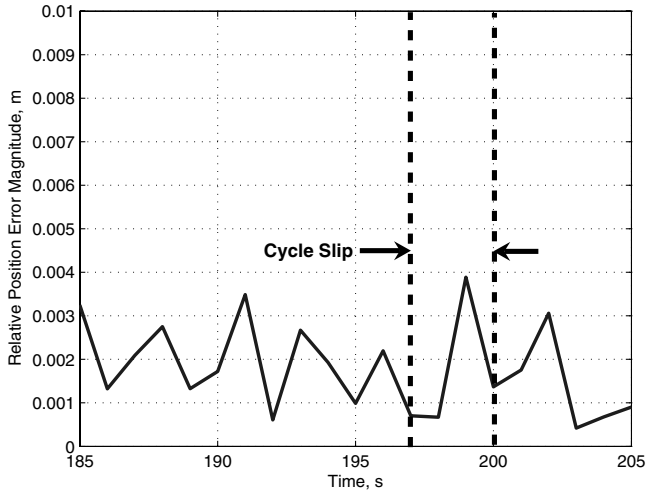

Fig. 10 Time history of the relative navigation error magnitude during a cycle slip event when using the new detection and recovery algorithm.

The algorithm, which uses an improved carrier-phase measurement model, reduces the measurement ambiguity search volume by using both pseudorange and carrier-phase measurements in the calculation of the solution and by imposing an integer condition on the double-differenced carrier-phase measurement ambiguities. The reduced search volume promotes rapid convergence to the correct ambiguities. The algorithm uses an efficient decorrelation and integer search scheme to rapidly calculate the correct ambiguities, and it employs a robust cycle slip detection and recovery system.

The new estimator can converge to the correct integer ambiguities in 1–2 one-second measurement steps in a 1-km-baseline LEO formation and can reach an ambiguity validation certainty of 99% in 3–4 measurement steps as determined by idealized hardware-in-the-loop tests. In off-line GEO simulations of a 3-km-baseline formation, the algorithm can converge to the correct integers in 1–2 30-second time steps and can reach an ambiguity validation certainty of 99% in 3–4 time steps. In off-line HEO simulations at a radial distance of 17.8 Earth radii, the estimator can converge to the correct integers in about 3 min and can reach a certainty of 99% in 9–10 30-second time steps. The convergence rates in GEO and HEO indicate that, with careful implementation, LAMBDA techniques can allow CDGPS techniques to be used in high-altitude formations with $L1$-only measurements.

The estimator achieves 3-dimensional relative position errors on the order of 3 mm over a 1 km baseline in LEO, 0.1 m over a 3 km baseline in GEO, and 3 m over a 10 km baseline at apogee in HEO. These relative navigation accuracies exceed those required for many formation flying missions. The results, however, rest on the assumption that error models in the off-line simulator are accurate. These models should be validated against real data when high-altitude, weak-signal data become available. Further improvement may be achieved by including dynamics models in the estimator, thus making it more robust to random errors.

The cycle slip detection and recovery system correctly detects carrier-phase measurement errors, identifies the slip channel, estimates the number of cycles slipped, and returns the proper a priori information to the executive estimator. It does so without degrading the relative navigation solution during the slip transient.

Acknowledgments

This work has been supported in part by a Graduate Student Researcher Program Fellowship administered through the NASA Goddard Space Flight Center with Russell Carpenter acting as Technical Advisor and in part by NASA Cooperative Agreement No. NCC5-722, which has been monitored by Michael C. Moreau. The authors would like to thank M. C. Moreau for facilitating the use of NASA's Formation Flying Testbed and Oliver Montenbruck of the German Aerospace Center for developing very capable, space-qualified receivers and for making his hardware-simulator data available to us.

References

[1] NASA, "Magnetospheric Multiscale Mission. . .Resolving Fundamental Processes in Space Plasmas," MSS Documents, NASA Doc. No. TM-2000-209883, 1999.

[2] Busse, F. D., How, J. P., and Simpson, J., "Demonstration of Adaptive Extended Kalman Filter for Low-Earth-Orbit Formation Estimation Using CDGPS," *Navigation: Journal of the Institute of Navigation*, Vol. 50, No. 2, 2003, pp. 79–94.

[3] Leung, S., and Montenbruck, O., "Real-Time Navigation of Formation-Flying Spacecraft Using-Global-Positioning-System Measurements," *Journal of Guidance, Control, and Dynamics*, Vol. 2, No. 6, Nov.–Dec. 2004, pp. 226–235.

[4] Wolfe, J., and Speyer, J. L., "Effective Estimation of Relative Position in Orbit Using Differential Carrier-Phase GPS," AIAA Paper 2004-4772, 2004.

[5] Kroes, R., and Montenbruck, O., "High Accuracy Kinematic Spacecraft Relative Positioning Using Dual-Frequency GPS Carrier Phase Data," *Proceedings of the 2004 ION NTM Conference*, Inst. of Navigation, Fairfax, VA, 26–28 Jan. 2004.

[6] Kroes, R., Montenbruck, O., Bertiger, W., and Visser, P., "Precise GRACE Baseline Determination Using GPS," *GPS Solutions*, Vol. 9, No. 1, April 2005, pp. 21–31.

[7] Psiaki, M. L., and Mohiuddin, S., "Global Positioning System Integer Ambiguity Resolution Using Factorized Least-Squares Techniques," *Journal of Guidance, Control, and Dynamics*, Vol. 30, No. 2, March–April 2007, pp. 346–356.

[8] Psiaki, M. L., and Mohiuddin, S., "Modeling, Measurement, and Simulation of GPS Carrier-Phase for Spacecraft Relative Navigation," *Proceedings of the AIAA Guidance, Navigation, and Control Conference*, AIAA, Reston, VA, 16–19 Aug. 2005.

[9] Gurtner, W., "RINEX-2.10 Format," http://www.ngs.noaa.gov/CORS/instructions2 [retrieved 29 Jan. 2005].

[10] Gill, P. E., Murray, W., and Wright, M. H., *Practical Optimization*, Academic Press, London, 2003, pp. 37–40.

[11] Bierman, G.J., *Factorization Methods for Discrete Sequential Estimation*, Academic Press, New York, 1977.

[12] Spirent Federal Systems, "GPS Simulator Products Overview," http://www.spirentfederal.com [retrieved 29 Jan. 2005].

[13] Montenbruck, O., Ebinuma, T., Lightsey, E. G., and Leung, S., "A Real-Time Kinematic GPS Sensor for Spacecraft Relative Navigation," *Aerospace Science and Technology*, Vol. 6, No. 6, 2002, pp. 435–449.

[14] Psiaki, M. L., "Block Acquisition of Weak GPS Signals in a Software Receiver," *Proceedings of the 2001 ION GPS Conference*, Inst. of Navigation, Fairfax, VA, 11–14 Sept. 2001, pp. 2838–2850.

[15] Psiaki, M. L., and Jung, H., "Extended Kalman Filter Methods for Tracking Weak GPS Signals," *Proceedings of the 2002 ION GPS Conference*, Inst. of Navigation, Fairfax, VA, 24–27 Sept. 2002, pp. 2539–2553.